J. Korean Inst. Electr. Electron. Mater. Eng.
Vol. 36, No. 2, pp. 175-185 March 2023
DOI: https://doi.org/10.4313/JKEM.2023.36.2.11
ISSN 1226-7945(Print), 2288-3258(Online)

Regular Paper

Self-Supporting 3D-Graphene/MnO_2 Composite Supercapacitors with High Stability

Zhaoyang Han and Sang-Hee Son

Department of System Semiconductor Engineering, Cheongju University, Cheongju 28503, Korea

(Received November 24, 2022; Revised January 7, 2023; Accepted January 11, 2023)

Abstract: A hybrid supercapacitor is a promising energy storage device in view of its excellent capacitive performance. Commercial three-dimensional foam nickel (Ni) can be used as an ideal framework due to an interconnected network structure. However, its application as an electrode material for supercapacitors is limited due to its low specific capacity. Herein, we report a successful growth of MnO_2 on the surface of graphene by a one-step hydrothermal method; thus, forming a three-dimensional MnO_2-graphene-Ni hybrid foam. Our results show that the mixed structure of MnO_2 with nanoflowers and nanorods grown on the graphene/Ni foam as a hybrid electrode delivers the maximum specific capacitance of 193 $F \cdot g^{-1}$ at a current density 0.1 $A \cdot g^{-1}$. More importantly, the hybrid electrode retains 104% of its initial capacitance after 1,000 charge-discharge cycles at 1 $A \cdot g^{-1}$; thus, showing the potential application as a stable supercapacitor electrode.

Keywords: Manganese dioxide, Graphene, Hydrothermal method, Heterojunction, Supercapacitors

1. INTRODUCTION

In the recent decades, renewable energy sources such as solar energy, wind energy, hydrogen energy, bioenergy, etc have gained considerable importance. Due to high-performance energy storage characteristics, a wide variety of energy storage devices, such as: solar cells, lithium-ion batteries, supercapacitorsetc have been developed which find wide applications in electric/hybrid vehicles, commercial wearable electronic devices, industrial electricity, and other aspects [1-3]. Among them, supercapacitors have become a hot research topic due to their advantages such as high power density, fast charging and discharging speed and excellent cycle stability [4]. Based on the mechanism of energy storage, the electrode materials of supercapacitors can be divided into two categories: (1) Transition metal oxides such as: nickel oxide, manganese dioxide, tin dioxide, ruthenium dioxide with pseudo-capacitance characteristics [5-8]. (2) Carbon-based materials such as: activated carbon, carbon nanotubes, graphene having electric double layer capacitance characteristics [9-11]. Among these electrode materials, manganese dioxide has attracted widespread attention due to its high theoretical specific capacitance (1,370 $F \cdot g^{-1}$), simple preparation process, environmental friendliness, and other characteristics [12]. However, low conductivity and complex crystal structure of manganese dioxide severely limit its electrode activity, and the specific capacitance obtained is much lower than the theoretical value [13].

In order to improve the conductivity and actual specific capacitance of manganese dioxide, researchers have followed two routes: (1) Preparation of α, β, γ, δ and other manganese dioxide electrode materials with various crystal structures using hydrothermal method, electrodeposition method,

✉ **Sang-Hee Son; shson@cju.ac.kr**

chemical and liquid phase method etc, and studying different electrochemical properties of these crystal structures [14-16]. (2) Using highly conductive activated carbon, carbon nanotubes, graphene, etc as the carrier of manganese dioxide to prepare a composite electrode of manganese dioxide and carbon-based materials having different nanostructures such as: nanoflower, nanorod, tubular and nanofiber, etc., and comparing their electrochemical properties [17-21]. In spite of the large number of manganese dioxide/carbon matrix composites being reported, fully balancing the electrochemical activity, conductivity and stability is still a challenging task.

In this manuscript, one-step hydrothermal method was used for the successful growth of various nanostructures of manganese dioxide on the three-dimensional graphene/foam nickel skeleton like nano-flower, mixture of nano-flower and nano-rod, and nano-rod-like structure to investigate the morphological effect in nanostructures. After systematic characterization of the manganese dioxide/graphene/foam nickel heterojunction electrode structure, the electrochemical properties of manganese dioxide/graphene/foam nickel heterojunction electrode were tested. The study found that when the hydrothermal reaction temperature was 120℃ and the hydrothermal reaction time was 1 h, the resulting manganese dioxide/graphene/foam nickel electrode showed the largest specific capacitance (193 $F \cdot g^{-1}$) and maintains excellent cycle stability, thus showing promise as a high-performance supercapacitor electrode material.

2. EXPERIMENTAL

2.1 Chemicals and materials

The chemical reagents involved in the experiments, such as polystyrene, absolute ethanol, acetone, polyethylene glycol, hydrochloric acid, sodium sulfate, potassium permanganate and etc were of analytical grade. The density of nickel foam used in the experiment was 0.38 g/cm^2, and the thickness was 1.6 mm.

2.2 Heterojunction preparation

Graphene/foam nickel heterojunction preparation: Nickel foam (1 cm × 3 cm × 1.6 mm) was ultrasonically cleaned by acetone, dilute hydrochloric acid and absolute ethanol successively for the removal of surface impurities before putting it into the oven for drying. Polystyrene was packed into glass container which was then sealed with tin foil, leaving small holes in the foil to produce hydrocarbons during the heating of polystyrene. With nickel foam as the catalyst base, it is placed in the middle of tube furnace where polystyrene behaves as the carbon source. The tubular furnace was 3 times pumped with a gas mixture of arg on and hydrogen having a volume ratio of 9:1 maintaining a gas flow rate of 400 sccm. After reacting at 1,000℃ for 10 min, the tubular furnace was naturally cooled down to obtain a heterojunction of graphene/nickel foam.

Manganese dioxide/graphene/foam nickel heterojunction preparation: 0.5 g of potassium permanganate and 0.2 g of polyethylene glycol were weighed into 40 mL deionized water which was then ultrasonically dispersed and stirred evenly and then the solution was transferred to a reactor having 50 mL capacity. Then the graphene/nickel foam prepared as above is placed into the reactor and two groups of comparative experiments were designed. In the first group of experiments, the hydrothermal reaction temperature was varied from 100, 120, 140 and 160℃ keeping 1 h as the hydrothermal reaction time. In the second group of experiments, the reaction time was varied at 0.5, 1 and 2 h, maintaining a constant hydrothermal reaction temperature of 120℃. After the completion of hydrothermal reaction, the obtained samples were naturally cooled, and washed repeatedly with deionized water, and then dried in an oven at 60℃ for 12 h.

2.3 Material characterization

The morphology of the samples was observed by field emission scanning electron microscope (SEM, Hitachi S-4800). X-ray diffractometer (XRD, Cu K light source, Bruker D8 Advance) in the angle range of 10~80° was employed to investigate structural parameters of the obtained samples. Raman spectra of the samples were measured using Renishaw Raman tester having laser wavelength of 532 nm. The intrinsic properties of the samples were characterized by X-ray photoelectron spectroscopy (XPS, K-Alpha 0.5 eV). The specific surface and porosity analyzer of American Konta Instrument Company model SI-MP was employed for carrying out the nitrogen adsorption and desorption test; The specific

surface area was determined by the fully automatic specific surface area method and the pore size distribution was calculated by a porosity analyzer.

2.4 Electrochemical performance test

The electrochemical test was carried out in an electrochemical workstation (CHI660) employing a three-electrode system, where an aqueous solution of 1 mol· L^{-1} Na_2SO_4 was used as the electrolyte, platinum sheet (1 cm × 1 cm) as the counter electrode, and Ag/AgCl as the reference electrode. As working electrode, 1 cm × 1 cm of the above prepared manganese dioxide/graphene/nickel foam heterojunction was directly used. The voltage range during the cyclic voltammetric (CV) measurements was -0.2 V to 0.8 V (vs Ag/AgCl) with sweep rates set to 5, 10, 30, 50 and 100 mV·s^{-1}. The voltage range of during the constant current charge and discharge (GCD) test, the voltage range was set at -0.2 V to 0.8 V (vs Ag/AgCl) with the current density set to 0.1, 0.3, 0.5, 1, 3 and 5 A·g^{-1}. The mass ratio capacitance of the supercapacitor electrode was calculated as follows: $C_m = I \times \Delta_t/(m \times \Delta V)$, where I is the constant current, Δt is the discharge time, m is total mass of the heterojunction electrode, and ΔV is the potential difference during discharge. Ac impedance test (EIS) was carried out in the frequency range of 100 kHz ~ 10 mHz and an AC amplitude of 5 mV.

3. RESULTS AND DISCUSSION

3.1 Microstructure characterization

The microscopic morphology of manganese dioxide/graphene/nickel foam heterojunction is shown in Fig. 1. The pleated structure of graphene thin film on the surface of nickel foam, as well as the manganese dioxide in graphene can be clearly seen from the figure. Various topography features of the surface can also be seen in the figure. For same hydrothermal reaction time, different morphologies of manganese dioxide nanostructures can be obtained at different hydrothermal reaction temperatures. For the hydrothermal reaction temperature of 100℃, Figs. 1(a), (b) show the distribution of a large number of nanoflower-like manganese dioxide on the surface of graphene. When the hydrothermal reaction temperature reached 120℃, in addition to nanoflower-like manganese dioxide, nanorod-like manganese dioxide are also distributed on the surface of graphene as can be seen in Figs. 1(c), (d). As evident from Figs. 1(e), (f), further increase of the hydrothermal reaction temperature to 140℃ resulted in the appearance of a large number of nanoflower-like and nanorod-like manganese dioxide aggregates on the surface of graphene. And when the hydrothermal reaction temperature increased to 160℃, the structure was composed of nanorod-like structure as shown by Figs. 1(g), (h) graphene. Therefore, the nanostructure of manganese dioxide on the surface of graphene can be seen to vary with the hydrothermal reaction temperature as evident

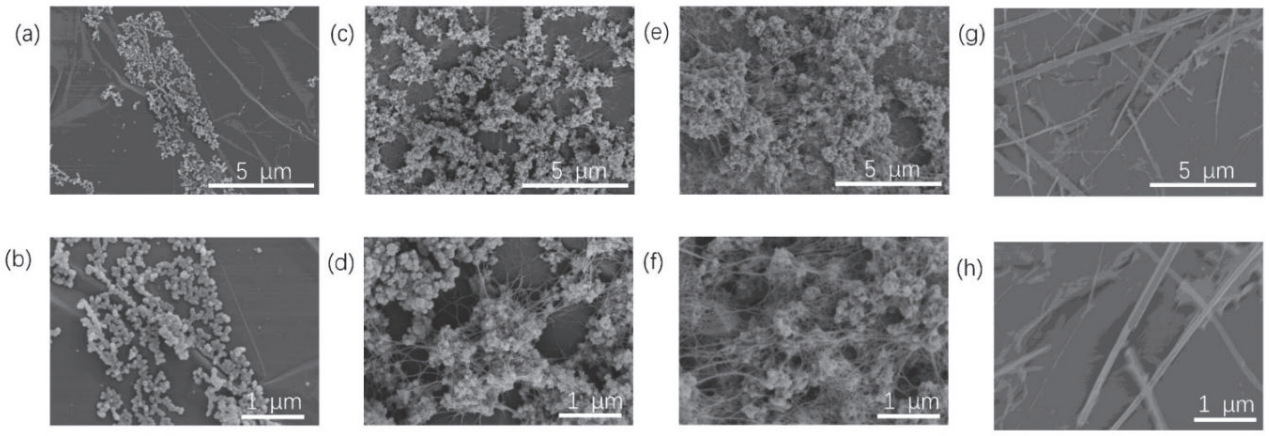

Fig. 1. SEM images of the MnO_2/graphene/Ni for the reaction time of 1 h corresponding to different growth temperature: (a, b) 100℃, (c, d) 120℃, (e, f) 140℃, and (g, h) 160℃.

from Fig. 1, changing from nanoflowers at low temperature to nanorods at high temperature. The change of crystal morphology is completely consistent with the Ostwald ripening mechanism of crystal growth [22-24]. The above experimental results are also consistent with our previous research results indicating change of morphology of manganese dioxide from nanoflowers to nanorods due to change of temperature under hydrothermal reaction conditions [25]. The difference is that in this experiment the growth of manganese dioxide is in the surface of graphene and due to the catalytic action of carbon the energy required for this morphological change is reduced, that is, the morphological change occurs at lower temperature. The equation is：

$$4KMnO_4 + 3C + H_2O \rightarrow 4KMnO_2 + K_2CO_3 \quad [25]$$

In addition, the morphology change of manganese dioxide on the graphene surface was also observed with changing time of hydrothermal reaction maintaining the hydrothermal reaction temperature constant at 120℃, as shown in Fig. 2. When the hydrothermal reaction time was half an hour (0.5 h), growth of a large amount of nanoflower-like manganese dioxide can be seen on the graphene surface as seen in Figs. 2(a), (b). Extending the hydrothermal reaction time to 1 hour showed the presence of both nanoflower-like and nanorod-like manganese dioxide on the graphene surface evident from Figs. 2(c), (d).

In addition, some purities like K, Ni and Al, which may be due to the presence of nickel foam, potassium permanganate solvent and other issues. Extending the hydrothermal reaction time to 2 h resulted in the accumulation of a large number of manganese dioxide nanoflowers and nanorods on the surface of graphene seen in Figs. 2(e), (f). This may be due to long reaction time, these manganese dioxide layers accumulate and get detached from the graphene surface. Although after a long hydrothermal reaction, nanorod-like manganese dioxide has been formed on the surface of graphene, there are still a large number of nanoflower-like manganese dioxide, which may be due to the low temperature of the hydrothermal reaction. Complete transformation of the nanoflower-like manganese dioxide into nanorod-like manganese dioxideis not possible [26].

Nickel foam-removed manganese dioxide/graphene heterojunction samples were transferred onto a micro-grid copper mesh for microstructural analysis by TEM [27]. Figure 3 shows the TEM image of the manganese dioxide/grapheme heterojunction prepared by hydrothermal reaction at 120℃ for 1 h. Figure 3(a) shows the distribution of manganese dioxide nanoflowers and nanorods in large areas of graphene surface. In Fig. 3(b), nanoflower-like manganese dioxide can be seen clearly seen adhering to the edges of graphene. The lattice spacing of the nanoflower surface as observed from the high-resolution TEM image shown in Fig. 3(c) is 0.26 nm [28]. The transmission electron microscopy elemental analysis of Fig.

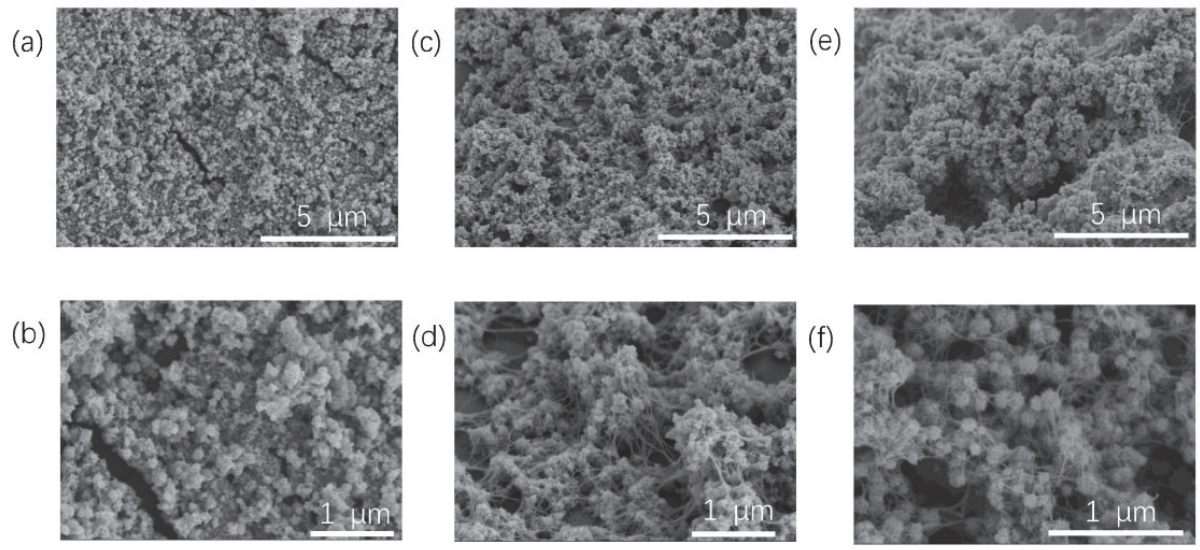

Fig. 2. SEM images of the MnO_2/graphene/Ni prepared at 120℃ for different growth time: (a, b) 0.5 h, (c, d) 1 h, and (e, f) 2 h.

3(d) shows uniform distribution of C but Mn and O are only obvious in the area where the nanoflowers gather, which fully demonstrates the formation of a heterojunction structure by manganese dioxide on the surface of graphene.

For more detailed analysis of the structure of manganese dioxide on the surface of graphene, Raman spectrum of the manganese dioxide/graphene heterojunction obtained by hydrothermal reaction at 120℃ for 1 hour was measured, as shown in Fig. 4(a). The peak corresponding to the region of 200~1,000 cm^{-1} is due to manganese dioxide, and the peaks in the region of 1,000~3,000 cm^{-1} is the peak due to graphene. In the high-frequency Raman spectrum, 2D and G bands were observed at ~2,680 cm^{-1} and ~1,590 cm^{-1}, respectively, while the D band at ~1,350 cm^{-1} was due to impurity defects and these peaks are originated due to the presence of graphene [29]. In the low-frequency region of the Raman spectrum, the sharp peak at ~640 cm^{-1} originates from the stretching vibration of Mo-O perpendicular to the [MnO_6] octahedron, and the peak at 507 cm^{-1} corresponds to the crystalline phase structure of nanoflower-like δ-MnO_2 [30]. The peak at ~380 cm^{-1} corresponds to the crystal structure of nanorod-like α-MnO_2 [31], and the peak at 613 cm^{-1} is similar to the tunnel structure of pyrolusite [32]. Presence of these spectral peaks indicates that the composite structure of nanoflowers and nanorods formed by manganese dioxide on the surface of graphene is consistent with the SEM morphology discussed

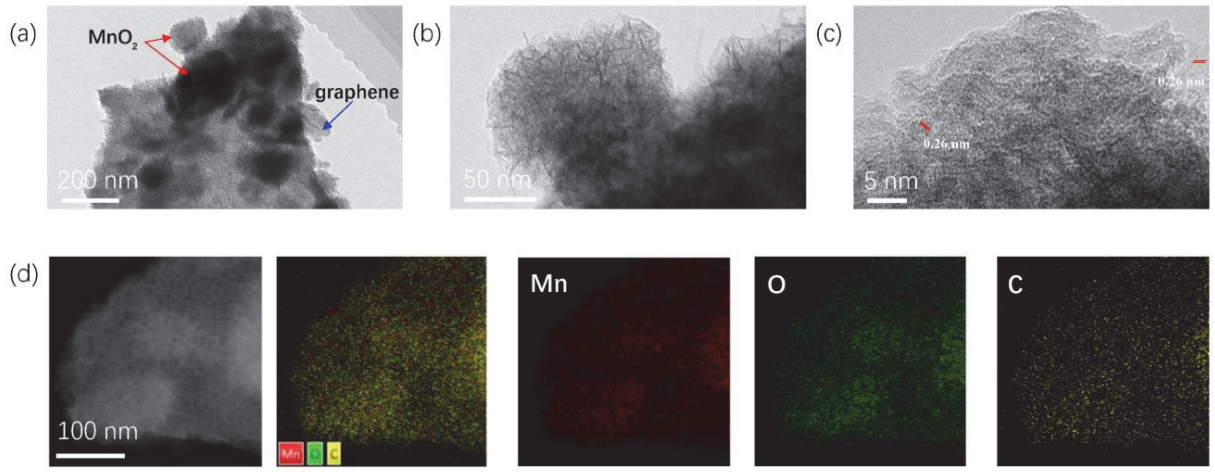

Fig. 3. (a-c) TEM images of the MnO_2/graphene at 120℃ for 1 h and (d) elemental mapping images.

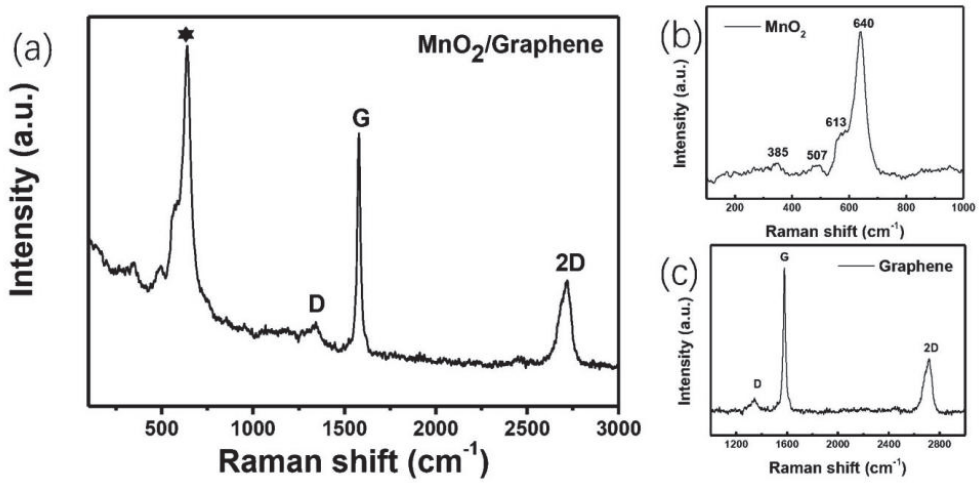

Fig. 4. Raman spectrum of the MnO_2/graphene/Ni at prepared at 120℃ for a reaction time of 1 h: (a) survey scan, (b) MnO_2, and (c) graphene Raman spectrums.

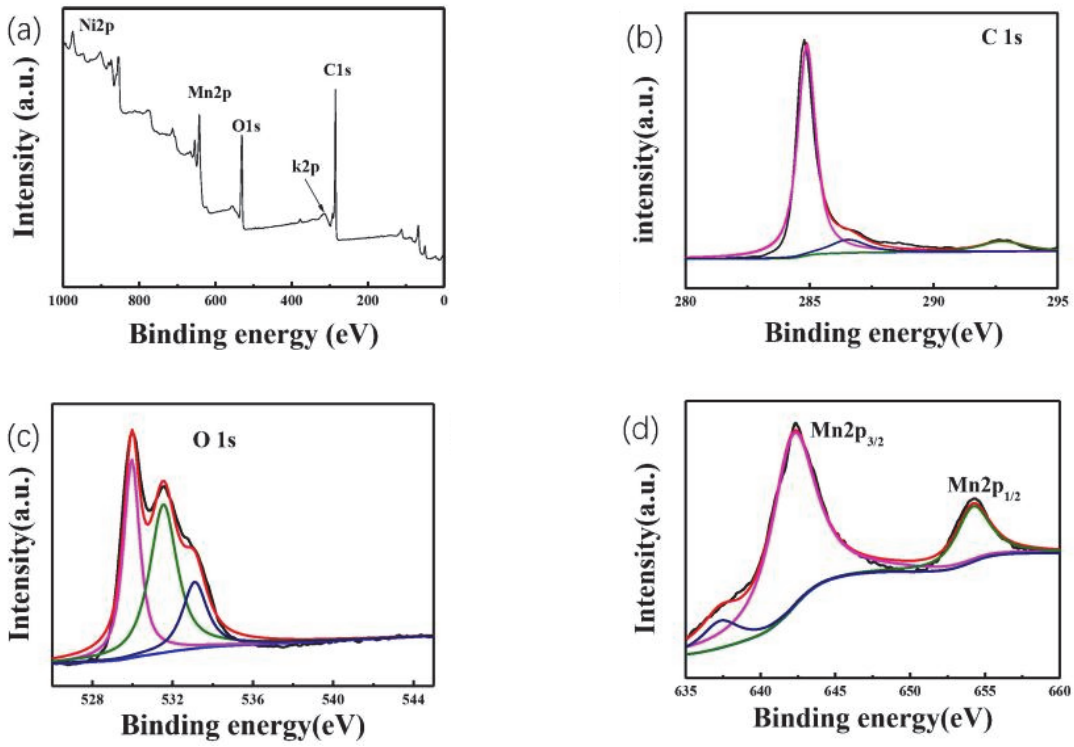

Fig. 5. XPS spectrum of the MnO_2/graphene prepared at 120℃ for a reaction time of 1 h: (a) survey scan, (b) C 1s, (c) O 1s, and (d) Mn 2p high-resolution spectrums.

earlier.

Figure 5 shows the XPS spectrum of the heterojunction formed on the surface of graphene by manganese dioxide corresponding to the hydrothermal reaction at 120℃ for 1 hour. In Fig. 5(a), the survey spectrum shows the presence of C, Mn, O, Ni and K elements in the sample. Figure 5(b) shows the deconvulated C1s spectrum, which is derived from the graphene film formed on the nickel foam. The C1s peak can be decomposed into four minor peaks: sp^2-C=C (284.5 eV), C-O (285.4 eV), C=O (286.7 eV, epoxy), and O-C=O (293.2 eV, carboxyl) [33]. The deconvulated O 1s peak shown in Fig. 5(c) is significantly different from that of the pure manganese dioxide prepared by hydrothermal method [25]. In addition to the normal oxygen peak at 532.0 eV (O-C), the other peak at 529.6 eV belongs to Mn-O of manganese dioxide [34]. The Mn 2p peak in Fig. 5(d) can be decomposed into two main sub-peaks corresponding to the binding energies of 642.6 eV and 653.9 eV belonging to Mn $2p_{3/2}$ and Mn $2p_{1/2}$, respectively. The spin energy gap is 11.3 eV, which further proves that manganese dioxide is formed on the surface of graphene [35].

Figure 6 shows determination of specific surface area, pore volume and pore size of the heterojunction formed on the

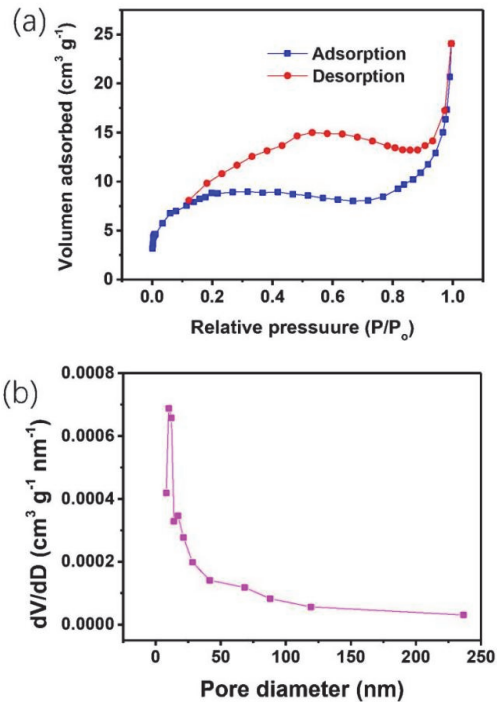

Fig. 6. Nitrogen adsorption-desorption isotherms (a) and corresponding pore size distributions (b) of the MnO_2/graphene samples prepared at 120℃ for a reaction time of 1 h.

surface of graphene after hydrothermal reaction of manganese dioxide at 120℃ for 1 hour. The nitrogen adsorption desorption curves of the nanoflower-like and nanorod-like composite structure of manganese dioxide formed on the surface of graphene are shown in Fig. 6(a). The blue and red curves correspond to the nitrogen adsorption and desorption process of the sample, respectively. The specific surface area calculated by the BET method was 29.65 $m^2 \cdot g^{-1}$. Through the BJH pore size distribution curve shown in Fig. 6(b), pore volume of the sample can be calculated to be 0.02 $cm^3 \cdot g^{-1}$ and the pore sizes were found to be distributed in the range of 4~20 nm. In general, large specific surface area and small pore size contribute to the diffusion of electrons and ions, resulting in better performance with respect to electrochemical energy storage [36].

3.2 Electrochemical performance test

No conductive agent or binder was needed to be added while using manganese dioxide/graphene/nickel foam heterojunction directly as working electrode for electrochemical performance test due to the unique self-supporting structure of nickel foam. Three different hydrothermal reaction times for 120℃ temperature were used to prepare the manganese dioxide/graphene/nickel foam heterojunctions based composite electrode used for testing the electrochemical performance: 0.5 h in Fig. 7(a), 1 h in Fig. 7(b) and 2 h in Fig. 7(c). For the CV curves of these heterojunctions, increasing the scanning rate from 5 $mV \cdot s^{-1}$ to 100 $mV \cdot s^{-1}$ does not change the symmetrical rectangular shape, though gradually increasing the area enclosed by the CV curve, indicating gradual increase of the corresponding capacity. However, increasing the scan rate to 100 $mV \cdot s^{-1}$ resulted in gradual deviation of the CV curve from the rectangular shape, indicating increasing pseudocapacitance contribution of manganese dioxide in addition to the double layer energy storage characteristics of graphene [37]. The variation of the CV curve for the heterojunction obtained after different hydrothermal reaction time for identical hydrothermal reaction temperature was compared for a scan rate of 5 $mV \cdot s^{-1}$. As shown in Fig. 7(d), extending the hydrothermal reaction time from half an hour (0.5 h) to 1 h resulted in an increase of the area enclosed by the CV curve indicating that the corresponding capacity also increases. It is

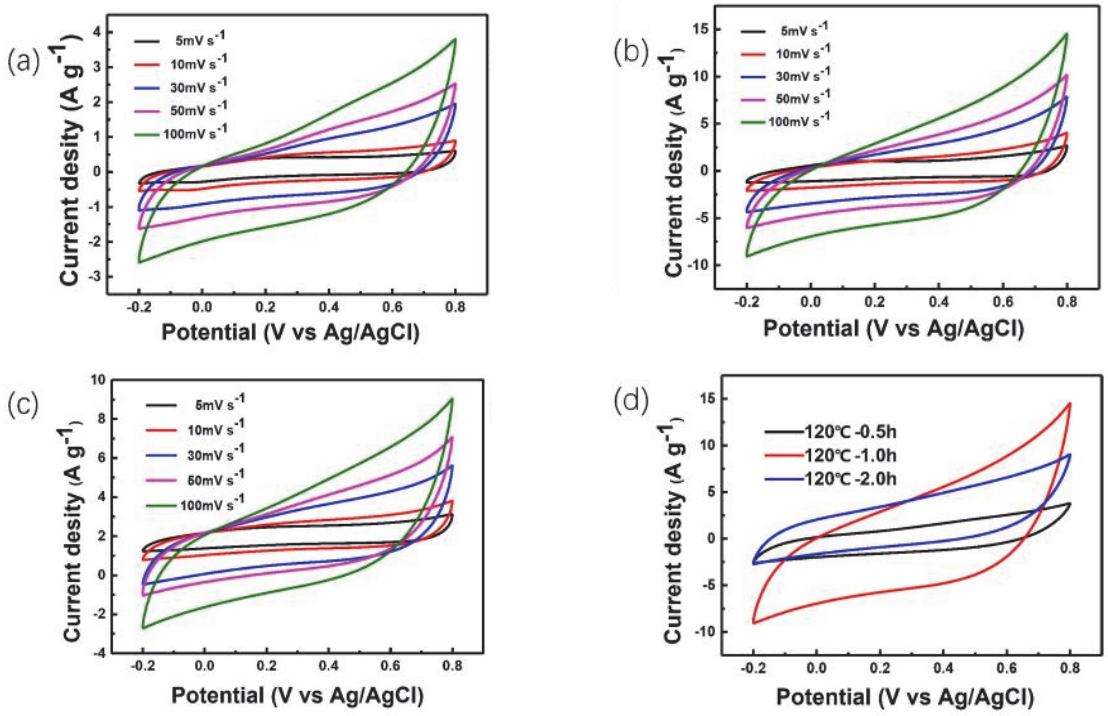

Fig. 7. CV curves at different scan rates (5~100 $mV \cdot s^{-1}$) for the MnO_2/graphene/Ni prepared at 120℃ for different reaction times of (a) 0.5 h, (b) 1 h, (c) 2 h, and (d) comparative CV curves at a scan rate of 5 $mV \cdot s^{-1}$.

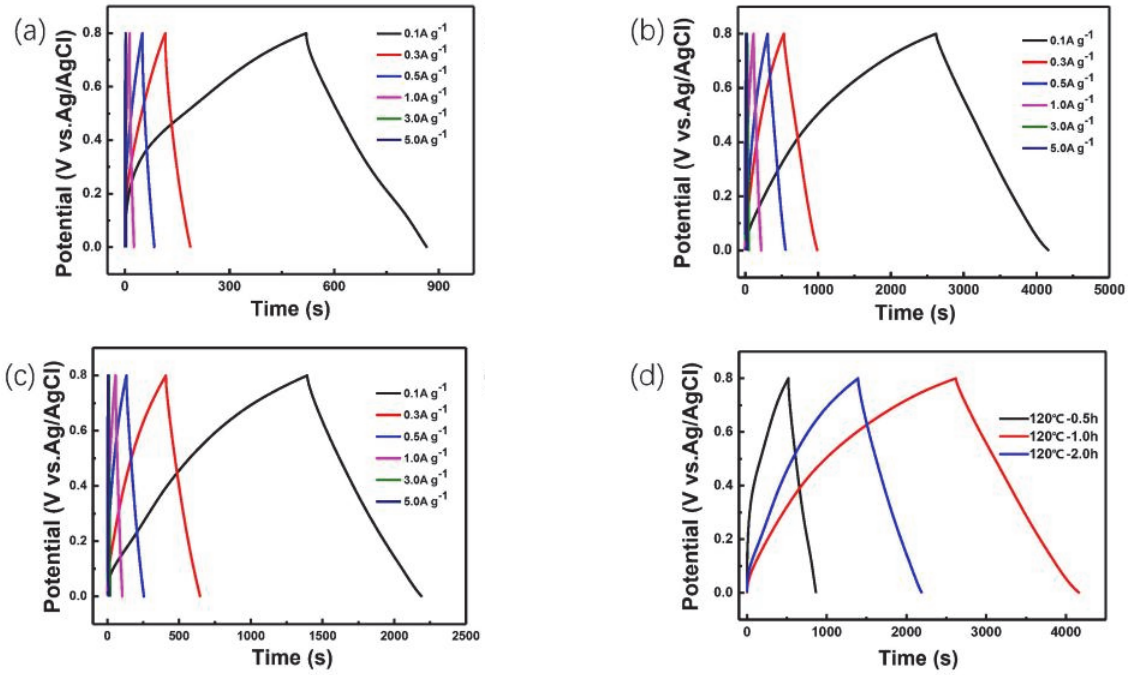

Fig. 8. GCD curves at different current densities (0.1~5 A·g^{-1}) for the MnO_2/graphene/Ni samples prepared at 120℃ for varying reaction time of (a) 0.5 h, (b) 1 h, (c) 2 h, and (d) comparative GCD curves at a current density of 0.1 A·g^{-1}.

worth noting that further extension of the hydrothermal reaction time to 2 h resulted in decreasing area under the CV curve compared to that for the CV corresponding to reaction time of 1 h, although it was still larger than that of the CV curve corresponding to 0.5 h, indicating that excessive manganese dioxide deposition may inhibit the efficiency of electrode [38]. In summary, the heterojunction electrode prepared by hydrothermal reaction at 120°C for 1 h has the highest charge storage performance.

In order to further investigate the effect of hydrothermal reaction time of manganese dioxide on the electrochemical performance of graphene, the constant current charge and discharge curves of the electrode were tested at different current densities. The GCD curves of three heterojunction electrodes at the current densities of 0.1, 0.3, 0.5, 1, 3, and 5 A·g^{-1} are shown in Figs. 8(a), (b), and (c), which correspond to the hydrothermal reaction times of 0.5 h, 1 h, and 2 h, respectively. All these curves show good triangular symmetry. Figure 8(d) shows the comparative GCD curves of the three heterojunction electrodes at the current density of 0.1 A·g^{-1}. The discharge time of the heterojunction electrode was the longest when the reaction time was 1 h, indicating highest capacity of the prepared electrode. Figure 9(a) compares the changes of mass specific capacitance of the manganese dioxide/graphene/nickel foam heterojunction electrode prepared by varying reaction time at different current densities. For 0.1 A·g^{-1} current density, extending the hydrothermal reaction time from 0.5 h to 1 h resulted in an increase of specific capacitance of the heterojunction electrode from 44 F·g^{-1} to 193 F·g^{-1}. But further extension of the hydrothermal reaction to 2 h resulted in the decrease of specific capacitance of the heterojunction electrode to 100 F·g^{-1}, which indicated that high loading of manganese dioxide on the surface of graphene led to a decrease in utilization efficiency of the electrode. However, the specific capacitance of the heterojunction electrode was still much larger than that of the heterojunction electrode initially loaded with manganese dioxide. In addition, Fig. 9(a) also shows that specific capacitance of the heterojunction electrodes prepared under three hydrothermal conditions shows good rate characteristics. The electrochemical impedance spectra of three heterojunction electrodes were studied as shown in Fig. 9(b) for testing the conductivity of the heterojunction electrodes. The solution resistance of three electrodes is almost the same as all three electrodes are self-supporting electrodes based on three-dimensional nickel foam skeleton and was tested in the same

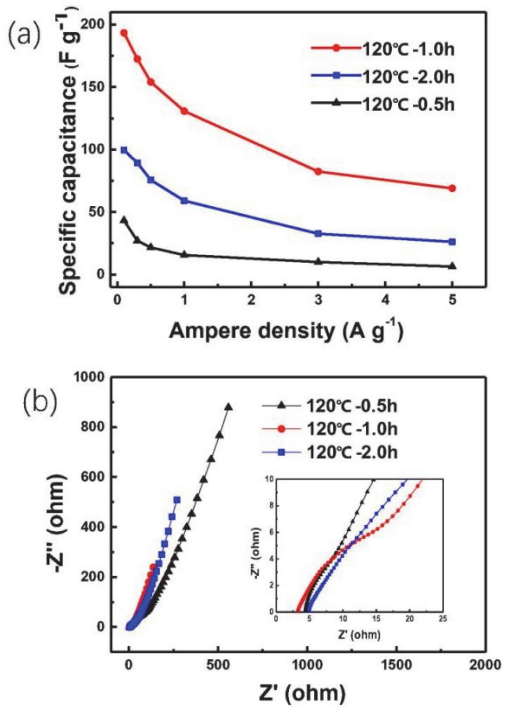

Fig. 9. Comparative specific capacitances (a) and EIS spectrums (b) of the MnO_2/graphene/Ni samples prepared at 120℃ with varying reaction time of 0.5 h, 1 h, and 2 h.

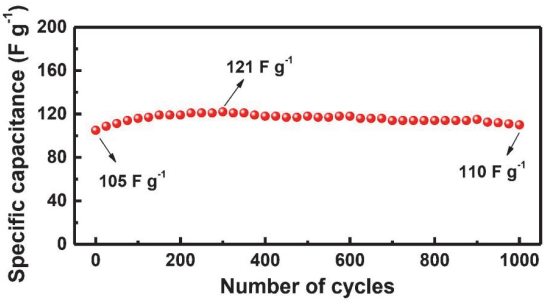

Fig. 10. The variation of specific capacitances of MnO_2/graphene/Ni prepared at 120℃ for 1 h as a function of cycle numbers during 1,000 GCD cycles at 1 A·g^{-1}.

electrolyte. However, different nanostructures of manganese dioxide on the surface of graphene result in different charge transfer resistance of the three electrodes, with the corresponding minimum (3.24 Ω) being obtained for the reaction time of 1 h. The charge transfer resistances corresponding to the reaction time of 0.5 h and 2 h were 4.36 and 4.85 Ω, respectively. This also shows that smaller the contact resistance, greater is the specific capacitance of the electrode [39].

In order to explore the electrochemical stability of the manganese dioxide/graphene/nickel foam heterojunction electrode, a constant current charge and discharge test was performed on the electrode at a current density of 1 A·g^{-1} for 1,000 times, as shown in Fig. 10. It can be seen that initially specific capacitance of the electrode was 105 F·g^{-1} which increased to 121 F·g^{-1} at 300 cycles, and the specific capacitance remained at 110 F·g^{-1} at 1,000 cycles. This may be due to the heterojunction electrode still maintaining an efficient ion transport channel after 1,000 cycles, so that the electrode can still reach a state of charge saturation after multiple cycles [40]. This fully demonstrates good electrochemical cycle stability of the manganese dioxide supercapacitor based on graphene heterojunction.

4. CONCLUSION

In this manuscript, graphene grown on the surface of three-dimensional nickel foam was used as the catalytic substrate, and manganese dioxide with various nanostructures was successfully prepared on the surface of graphene by one-step hydrothermal method. Manganese dioxide/graphene/nickel foam was used as a self-supporting electrode to study its electrochemical performance. In the early stage of hydrothermal reaction, nucleation of manganese dioxide occurred on the surface of graphene and chemical reaction started to occur gradually with increasing hydrothermal reaction temperature. First, nano-flower-like manganese dioxide was formed, which was then converted into nano-flower-like and nanorod-like mixed manganese dioxide. Finally, nanorod-like manganese dioxide was formed, which realized the effective regulation of manganese dioxide nanocrystal structure. By changing the hydrothermal reaction time, the manganese dioxide/graphene/nickel foam heterojunction electrode showed varying electrochemical behavior. Maximum mass specific capacitance of 193 F·g^{-1} (current density is 0.1 A·g^{-1}) was obtained when the hydrothermal reaction time was 1 h at a reaction temperature of 120°C. After 1,000 constant current charge and discharge cycles, it still maintains 100% of the initial capacity, showing great potential application value as an electrode material for supercapacitors.

ORCID

Sang-Hee Son http://orcid.org/0000-0003-4392-066X

ACKNOWLEDGEMENT

This paper was supported by Korea Institute for Advancement of Technology (KIAT) grant funded by the Korea Government (MOTIE) (P0017011, HRD Program for Industrial Innovation).

REFERENCES

[1] Y. T. Kim. *J. Korean Inst. Electr. Electron. Mater. Eng.*, **22**, 532 (2009). [DOI: https://doi.org/10.4313/JKEM.2009.22.6.532]

[2] D. H. Lee, K. M. Lee, and J. R. Yoon, *J. Korean Inst. Electr. Electron. Mater. Eng.*, **23**, 843 (2010). [DOI: https://doi.org/10.4313/JKEM.2010.23.11.843]

[3] J. H. Sul, I. K.You, S. H. Kang, B. N. Kim, and I. G. Kim, *J. Korean Inst. Electr. Electron. Mater. Eng.*, **31**, 102 (2018). [DOI: https://doi.org/10.4313/JKEM.2018.31.2.102]

[4] J. H. Choi, C. Lee, S. Cho, G. D. Moon, B. S. Kim, H. Chang, and H. D. Jang, *Carbon*, **132**, 16 (2018). [DOI: https://doi.org/10.1016/j.carbon.2018.01.105]

[5] Y. Wang, B. Chang, D. Guan, K. Pei, Z. Chen, M. Yang, and X. Dong, *Mater. Lett.*, **135**, 172 (2014). [DOI: https://doi.org/10.1016/j.matlet.2014.07.150]

[6] M. Shen, Y. Wang, and Y. X. Zhang, *Dalton Trans.*, **49**, 17552 (2020). [DOI: https://doi.org/10.1039/D0DT02733B]

[7] T. Kim, E. P. Samuel, C. Park, Y. I. Kim, A. Aldalbahi, F. Alotaibi, and S. S. Yoon, *J. Alloys Compd.*, **108**, 356 (2020). [DOI: https://doi.org/j.jallcom.2020.157902]

[8] P. Wang, H. Liu, Y. Xu, Y. Chen, J. Yang, and Q. Tan, *Electrochim. Acta*, **194**, 211 (2016). [DOI: https://doi.org/10.1016/j.electacta.2016.02.089]

[9] W. Sun, S. M. Lipka, C. Swartz, D. Williams, and F. Q. Yang, *Carbon*, **103**, 181 (2016). [DOI: https://doi.org/10.1016/j.carbon.2016.02.090]

[10] C. Wang, F. Li, H. Qu, Y. Wang, X. Yi, Y. Qiu, Z. Zou, Y. Luo, and B. Yu, *Electrochim. Acta*, **158**, 35 (2015). [DOI: https://doi.org/10.1016/j.electacta.2015.01.112]

[11] S. Witomska, Z. Liu, W. Czepa, A. Aliprandi, D. Pakulski, P. Pawluć, A. Ciesielski, and P. Samorì, *J. Am. Chem. Soc.*, **141**, 482 (2019). [DOI: https://doi.org/10.1021/jacs.8b11181]

[12] W. Wei, X. Cui, W. Chen, and D. G. Ivey, *Chem. Soc. Rev.*, **40**, 1697 (2011). [DOI: https://doi.org/10.1039/C0CS00127A]

[13] Y. Huang, Y. Li, Z. Hu, G. Wei, J. Guo, and J. Liu, *J. Mater. Chem. A*, **1**, 9809 (2013). [DOI: https://doi.org/10.1039/C3TA12148H]

[14] Q. Zhao, A. Song, S. Ding, R. Qin, Y. Cui, S. Li, and F. Pan, *Adv. Mater.*, **32**, 2002450 (2020). [DOI: https://doi.org/10.1002/adma.202002450]

[15] Y. Wang, W. Zhou, Q. Kang, J. Chen, Y. Li, X. Feng, D. Wang, Y. Ma, and W. Huang, *ACS Appl. Mater. Interfaces*, **10**, 27001 (2018). [DOI: https://doi.org/10.1021/acsami.8b06710]

[16] R. S. Kalubarme, H. S. Jadhav, and C. J. Park, *Electrochim. Acta*, **87**, 457 (2013). [DOI: https://doi.org/10.1016/j.electacta.2012.09.081]

[17] Y. Wang, W. Huo, X. Yuan, and Y. Zhang, *Acta Phys.-Chim. Sin.*, **36**, 1904007 (2020). [DOI: https://doi.org/10.3866/PKU.WHXB201904007]

[18] X. L. Bai, Y. L. Gao, Z. Y. Gao, J. Y. Ma, X. L. Tong, H. B. Sun, and J. A. Wang, *Appl. Phys. Lett.*, **117**, 183901 (2020). [DOI: https://doi.org/10.1063/5.0018708]

[19] S. B. Hong, J. M. Jeong, H. G. Kang, D. Seo, Y. Cha, H. Jeon, G. Y. Lee, M. Irshad, D. H. Kim, S. Y. Hwang, J. W. Kim, and B. G. Choi, *ACS Appl. Mater. Interfaces*, **10**, 35250 (2018). [DOI: https://doi.org/10.1021/acsami.8b12894]

[20] S. H. Patil, A. P. Gaikwad, B. J. Waghmode, S. D. Sathaye, and K. R. Patil, *New J. Chem.*, **44**, 6853 (2020). [DOI: https://doi.org/10.1039/C9NJ05898B]

[21] C. Zhu, X. Dong, X. Mei, M. Gao, K. Wang, and D. Zhao, *J. Mater. Sci.*, **55**, 17108 (2020). [DOI: https://doi.org/10.1007/s10853-020-05212-2]

[22] G. Li, Y. Lu, C. Lu, M. Zhu, C. Zhai, Y. Du, and P. Yang, *J. Hazard. Mater.*, **294**, 201 (2015). [DOI: https://doi.org/10.1016/j.jhazmat.2015.03.045]

[23] B. Li, G. Rong, Y. Xie, L. Huang, and C. Feng, *Inorg. Chem.*, **45**, 6404 (2006). [DOI: https://doi.org/10.1021/ic0606274]

[24] Y. P. Li and Y. Z. Hao, *Acta Phys.-Chim. Sin.*, **26**, 3365 (2010). [DOI: https://doi.org/10.3866/PKU.WHXB20101205]

[25] X. Bai, X. Tong, Y. Gao, W. Zhu, C. Fu, J. Ma, T. Tan, C. Wang, Y. Luo, and H. Sun, *Electrochim. Acta*, **281**, 525 (2018). [DOI: https://doi.org/10.1016/j.electacta.2018.06.003]

[26] J. Yan, Z. Fan, T. Wei, W. Qian, M. Zhang, and F. Wei, *Carbon*, **48**, 3825 (2010). [DOI: https://doi.org/10.1016/j.carbon.2010.06.047]

[27] G. Zhu, Z. He, J. Chen, J. Zhao, X. Feng, Y. Ma, Q. Fan, L. Wang, and W. Huang, *Nanoscale*, **6**, 1079 (2014). [DOI: https://doi.org/10.1039/c3nr04495e]

[28] M. T. Sun, B. C. Huang, J. W. Ma, S. H. Li, and L. F. Dong, *Acta Phys.-Chim. Sin.*, **32**, 1501 (2016). [DOI: https://doi.org/10.3866/PKU.WHXB201603171]

[29] H. Sun, J. Xu, C. Wang, G. Ge, Y. Jia, J. Liu, F. Song, and J. Wan, *Carbon*, **108**, 356 (2016). [DOI: https://doi.org/10.1016/j.carbon.2016.07.027]

[30] J. Y. Tang, P. Q. Cao, Y. B. Fu, P. H. Li, and X. H. Ma, *Acta Phys.-Chim. Sin.*, **30**, 1876 (2014). [DOI: https://doi.org/10.3866/PKU.WHXB201407172]

[31] M. Sun, B. Lan, L. Yu, F. Ye, W. Song, J. He, G. Diao, and Y. Zheng, *Mater. Lett.*, **86**, 18 (2012). [DOI: https://doi.org/10.1016/j.matlet.2012.07.011]

[32] S. Liang, F. Teng, G. Bulgan, R. Zong, and Y. Zhu, *J. Phys. Chem. C*, **112**, 5307 (2008). [DOI: https://doi.org/10.1021/jp0774995]

[33] U. M. Patil, J. S. Sohn, S. B. Kulkarni, H. G. Park, Y. Jung, K. V. Gurav, J. H. Kim, and S. C. Jun, *Mater. Lett.*, **119**, 135 (2014). [DOI: https://doi.org/10.1016/j.matlet.2013.12.105]

[34] Z. S. Wu, W. Ren, D. W. Wang, F. Li, B. Liu, and H. M. Cheng, *ACS Nano*, **4**, 5835 (2010). [DOI: https://doi.org/10.1021/nn101754k]

[35] S. Sun, P. Wang, S. Wang, Q. Wu, and S. Fang, *Mater. Lett.*, **145**, 141 (2015). [DOI: https://doi.org/10.1016/j.matlet.2015.01.061]

[36] J. Zhu, Y. Xu, J. Hu, L. P. Wei, J. Liu, and M. Zheng, *J. Power Sources*, **393**, 135 (2018). [DOI: https://doi.org/10.1016/j.jpowsour.2018.05.022]

[37] X. Dong, X. Wang, J. Wang, H. Song, X. Li, L. Wang, M. B. Chan-Park, C. M. Li, and P. Chen, *Carbon.*, **50**, 4865 (2012). [DOI: https://doi.org/10.1016/j.carbon.2012.06.014]

[38] X. Liang,Y. Jia, Z. Liu, and Z. Lei, *Acta Phys.-Chim. Sin.*, **36**, 1903034 (2020). [DOI: https://doi.org/10.3866/PKU.WHXB201903034]

[39] R. Xue, J. W. Yan, Y. Tian, and B. L. Yi, *Acta Phys.-Chim. Sin.*, **27**, 2340 (2011). [DOI: https://doi.org/10.3866/PKU.WHXB20111002]

[40] B. Li, Z. Li, Q. Pang, Q. Zhuang, J. Zhu, P. Tsiakaras, and P. K. Shen, *Electrochim. Acta*, **324**, 134878 (2019). [DOI: https://doi.org/10.1016/j.electacta.2019.134878]